Acta Crystallographica Section B
Structural Science
ISSN 0108-7681

Characterization of the pressure-induced second-order phase transition in the mixed-valence vanadate BaV_6O_{11}

Karen Friese,[a]* Yasushi Kanke[b] and Andrzej Grzechnik[a]

[a]Departamento Física Materia Condensada, Facultad de Ciencia y Tecnología, Universidad del País Vasco, Apdo 644, 48080 Bilbao, Spain, and [b]Advanced Nano Materials Laboratory, National Institute for Materials Science, 1-1 Namiki, Tsukuba, Ibaraki 305-0044, Japan

Correspondence e-mail: karen.friese@ehu.es

Received 27 February 2009
Accepted 17 April 2009

The pressure dependence of the structure of the mixed-valence vanadate BaV_6O_{11} was studied with single-crystal X-ray diffraction in a diamond–anvil cell. The compressibility data could be fitted with a Murnaghan equation of state with the zero-pressure bulk modulus $B_0 = 161$ (7) GPa and the unit-cell volume at ambient pressure = 387.1 (3) Å^3 ($B' = 4.00$). A phase transition involving a symmetry reduction from $P6_3/mmc$ to $P6_3mc$ can be reliably detected in the high-pressure data. The estimated transition pressure lies in the range $1.18 < P_c < 3.09$ GPa. The transition leads to a breaking of the regular Kagomé net formed by part of the V ions. While in the ambient pressure structure all V—V distances in the Kagomé net are equal, they split into inter-trimer and intra-trimer distances in the high-pressure phase. In general, these changes are comparable to those observed in the corresponding low-temperature transition. However, the pressure-induced transition takes place at a lower unit-cell volume compared with the temperature-induced transition. Furthermore, overall trends for inter-trimer and intra-trimer V—V distances as a function of the unit-cell volume are clearly different for datapoints obtained by variation of pressure and temperature. The behavior of BaV_6O_{11} is compared with that of NaV_6O_{11}. While in the latter compound the transition can be explained as a pure volume effect, in BaV_6O_{11} an additional degree of freedom related to the valence distribution among the symmetrically independent vanadium sites has to be taken into account.

1. Introduction

Most of the reported pressure-induced phase transitions involve a discontinuous change of the lattice parameters and/or a change of the crystal system. Thus, they are usually detected in X-ray diffraction by a pronounced shift of the reflection positions or/and by a splitting of certain groups of reflections. On the other hand, transitions involving a symmetry reduction within the same diffraction class which are not accompanied by the appearance of additional reflections are more difficult to detect as they are exclusively reflected in changes of intensities in the diffraction diagrams.

The observation of such a type of transition in high-pressure powder diffraction experiments is very difficult and has rarely been reported. Single-crystal diffraction, however, should be suitable for the study of these transitions provided the data are of sufficient quality. However, it remains to be seen how reliable a transition of this type can be characterized from high-pressure diffraction data.

A good system to study in this context is the family of mixed-valence vanadate compounds with the general composition AV_6O_{11} (A = Na, K, Sr, Pb, Ba) and structures

Table 1
Crystal data and experimental details for BaV_6O_{11} at the various pressures.

	(I), 0.0001 GPa	(II), 1.18 GPa	(III), 2.19 GPa	(IV), 3.09 GPa
Crystal data				
Chemical formula	BaV_6O_{11}	BaV_6O_{11}	BaV_6O_{11}	BaV_6O_{11}
M_r	619	619	619	619
Crystal system, space group	Hexagonal, $P6_3/mmc$	Hexagonal, $P6_3/mmc$	Hexagonal, $P6_3mc$	Hexagonal, $P6_3mc$
Temperature (K)	293	293	293	293
a, c (Å)	5.797 (3), 13.301 (3)	5.785 (3), 13.266 (4)	5.775 (3), 13.238 (4)	5.763 (3), 13.206 (4)
V (Å^3)	387.1 (3)	384.5 (3)	382.3 (3)	379.8 (3)
Z	2	2	2	2
Radiation type	Mo $K\alpha$	Mo $K\alpha$	Mo $K\alpha$	Mo $K\alpha$
μ (mm^{-1})	11.99	12.07	12.14	12.22
Crystal form, size (mm)	Prismatic, 0.1 × 0.08 × 0.06	Prismatic, 0.1 × 0.08 × 0.06	Prismatic, 0.1 × 0.08 × 0.06	Prismatic, 0.1 × 0.08 × 0.06
Data collection				
Diffractometer	Stoe IPDS-2T	Stoe IPDS-2T	Stoe IPDS-2T	–
Data collection method	ω scans	ω scans	ω scans	–
Absorption correction	Numerical	Numerical	Numerical	Numerical
T_{min}	0.176	0.172	0.173	0.173
T_{max}	0.218	0.218	0.218	0.219
No. of measured, independent and observed reflections	1209, 139, 102	1189, 164, 84	1016, 229, 108	1486, 283, 140
Criterion for observed reflections	$I > 3\sigma(I)$	$I > 3\sigma(I)$	$I > 3\sigma(I)$	$I > 3\sigma(I)$
R_{int}	0.063	0.065	0.062	0.08
θ_{max} (°)	28.4	28.5	28.0	28.0
Refinement				
Refinement on	F	F	F	F
$R[F^2 > 2\sigma(F^2)]$, $wR(F^2)$, S	0.037, 0.031, 1.39	0.032, 0.032, 1.02	0.028, 0.025, 0.75	0.027, 0.027, 0.77
No. of reflections	139	164	229	283
No. of parameters	13	13	17	17
$(\Delta/\sigma)_{max}$	0.001	0.001	0.007	0.001
$\Delta\rho_{max}$, $\Delta\rho_{min}$ (e Å^{-3})	1.66, −2.13	2.05, −2.78	2.69, −1.92	0.89, −0.85
Extinction method	None	None	None	None

	(V), 3.98 GPa	(VI), 4.62 GPa	(VII), 5.82 GPa
Crystal data			
Chemical formula	BaV_6O_{11}	BaV_6O_{11}	BaV_6O_{11}
M_r	619	619	619
Crystal system, space group	Hexagonal, $P6_3mc$	Hexagonal, $P6_3mc$	Hexagonal, $P6_3mc$
Temperature (K)	293	293	293
a, c (Å)	5.754 (3), 13.182 (4)	5.746 (3), 13.160 (4)	5.739 (4), 13.144 (4)
V (Å^3)	378.0 (3)	376.3 (3)	374.9 (4)
Z	2	2	2
Radiation type	Mo $K\alpha$	Mo $K\alpha$	Mo $K\alpha$
μ (mm^{-1})	12.28	12.34	12.38
Crystal form, size (mm)	Prismatic, 0.1 × 0.08 × 0.06	Prismatic, 0.1 × 0.08 × 0.06	Prismatic, 0.1 × 0.08 × 0.06
Data collection			
Diffractometer	Stoe IPDS-2T	Stoe IPDS-2T	Stoe IPDS-2T
Data collection method	ω scans	ω scans	ω scans
Absorption correction	Numerical	Numerical	Numerical
T_{min}	0.173	0.174	0.177
T_{max}	0.216	0.219	0.219
No. of measured, independent and observed reflections	1506, 255, 150	1919, 319, 179	1534, 292, 128
Criterion for observed reflections	$I > 3\sigma(I)$	$I > 3\sigma(I)$	$I > 3\sigma(I)$
R_{int}	0.069	0.072	0.083
θ_{max} (°)	26.5	28.1	28.4
Refinement			
Refinement on	F	F	F
$R[F^2 > 2\sigma(F^2)]$, $wR(F^2)$, S	0.032, 0.028, 0.95	0.031, 0.028, 0.92	0.027, 0.027, 0.69
No. of reflections	255	319	292
No. of parameters	17	17	17
$(\Delta/\sigma)_{max}$	0.001	0.002	0.001
$\Delta\rho_{max}$, $\Delta\rho_{min}$ (e Å^{-3})	1.17, −0.77	0.91, −0.85	1.61, −1.41
Extinction method	None	None	None

Computer programs used: *X-AREA* (Stoe & Cie, 2006), *JANA*2006 (Petříček *et al.*, 2006), *Absorb* (Angel, 2006).

related to the magnetoplumbite type (de Roy *et al.*, 1987; Kanke *et al.*, 1991; Mentre & Abraham, 1996; Kanke, 1999; Friese & Kanke, 2006). These compounds are of special interest owing to their magnetic and electrical properties (see references 5–23 in Friese & Kanke, 2006).

All compounds show at least one temperature-induced transition in which the symmetry is reduced from $P6_3/mmc$ to $P6_3mc$ (Kanke *et al.*, 1994; Akiba *et al.*, 1998; Kato *et al.*, 2001; Kanke, 1999; Hata *et al.*, 1999; Mentre *et al.*, 2001; Friese & Kanke, 2006). In an earlier study we already reported on a high-pressure single-crystal diffraction study on NaV_6O_{11} (Grzechnik *et al.*, 2008) and we detected a pressure-induced hexagonal–hexagonal transition equivalent to the one observed at low temperatures.

Here we present a comparable high-pressure study on BaV_6O_{11}, where, in principle, we expect to find similar phenomena. However, one has to bear in mind that the charges of the *A* cation in NaV_6O_{11} and BaV_6O_{11} are different and, as a result, the valence states of vanadium, $3V^{3+}$ and $3V^{4+}$ in the first compound compared with $4V^{3+}$ and $2V^{4+}$ in the second, are different.

The aim of this study is twofold: on one hand we aim to know how reliably a transition involving a point group reduction within the same crystal system can be characterized from high-pressure data and what the limits of the information contents are.

On the other hand, we are interested in the high-pressure behaviour of BaV_6O_{11}. In particular, our interest is centered on how the high-pressure behaviour compares with that observed at low temperatures. Furthermore, we are interested in the influence that the incorporation of differently charged *A* cations in BaV_6O_{11} and NaV_6O_{11} has on the low-temperature and high-pressure behaviour of representatives of the AV_6O_{11} family of compounds.

2. Experimental details and structure determination

2.1. Data acquisition

The single crystals of BaV_6O_{11} were synthesized under high pressure according to the procedure described in Kanke (1999) and Friese & Kanke (2006). Single-crystal diffraction experiments were carried out *in situ* using a diamond–anvil cell of the Almax type (Boehler, 2006; Boehler & de Hantsetters, 2004) providing large opening angles of $2\theta = 80^\circ$. The approximate size of the crystal was $60 \times 60 \times 100$ µm. Diffraction data were measured on a Stoe IPDS-2T diffractometer. Multiple runs at two different 2θ positions of 0 and 15° of the imaging-plate detector were measured at each pressure point. The diamond cell was pre-centered optically. The centering was checked through the comparison of the orientation matrices corresponding to individual runs. A 1:1 mixture of pentane and isopentane, which is hydrostatic up to 7.4 GPa (Piermarini *et al.*, 1973) and does not react with the sample, was used as a pressure medium. For pressure calibration the ruby luminescence method was employed. The error in pressure determination was 0.02 GPa.

Regions on the imaging plate shadowed by the diamond–anvil cell were masked prior to integration. Integration was carried out using three orientation matrices simultaneously, one belonging to the sample, the other two corresponding to the two diamonds of the high-pressure cell. This way sample reflections overlapping with diamond reflections were excluded to a high degree during the integration procedure. Both the masking procedure and the simultaneous integration using multiple orientation matrices are provided in the *X-AREA* software (Stoe & Cie, 2006).

Reflections of both runs were averaged using the program *JANA*2006 (Petříček *et al.*, 2006). Outlying individual reflections with $I - I(\text{average}) > 10\sigma[I(\text{average})]$ were identified from the corresponding listing in *JANA*2006 and then cross-checked on the original frames using the *X-AREA* software (Stoe & Cie, 2006). They were excluded from the datasets if:

(i) they were lying in the tail of diamond reflections,

(ii) they were very close to the masked regions and could be assumed to be partly in the shadow of the diamond–anvil cell,

(iii) they were lying on or very close to the strongest gasket diffraction rings.

The varying number of measured reflections as shown in Table 1 is mainly due to the different degree of overlap of sample reflections with the powder rings of the gasket at the individual pressure points. In addition, with increasing pressure the thickness of the gasket decreases, leading, in general, to a considerable reduction of the background and consequently to a smaller number of reflections with falsified intensities.

Data were corrected for absorption by the diamonds with the program *Absorb* (Angel, 2006) and an empirical absorption correction for the crystal shape was applied using the program *JANA*2006 (Petříček *et al.*, 2006). The faces of the crystal were optimized with the program *X-shape* (Stoe & Cie, 1999).

2.2. Structure refinement

The structure refinement was started from the model coordinates of the room-temperature/ambient-pressure phase of BaV_6O_{11} (Friese & Kanke, 2006). All atoms were treated isotropically.[1] Three models were refined for all pressures.

Model 1: space group $P6_3/mmc$; 13 parameters. No additional restrictions were applied to coordinates or displacement parameters.

Model 2: space group $P6_3mc$; 17 parameters. While the coordinates of Ba and V ions were allowed to refine freely, the coordinates of the O atoms were restrained to be in accordance with the high-symmetry phase. Displacement parameters of atoms related *via* the mirror plane of the space group $P6_3/mmc$ (V2*a*/V2*b*; O1*a*/O1*b*; O3*a*/O3*b*) were restrained to be equal to avoid unnecessary correlations.

[1] Trial refinements with anisotropic displacement parameters led to reasonable values for all atoms. However, as the number of parameters in the refinement is increased considerably when compared with an isotropic refinement and as the overall agreement factors did not improve significantly, these refinements were discarded.

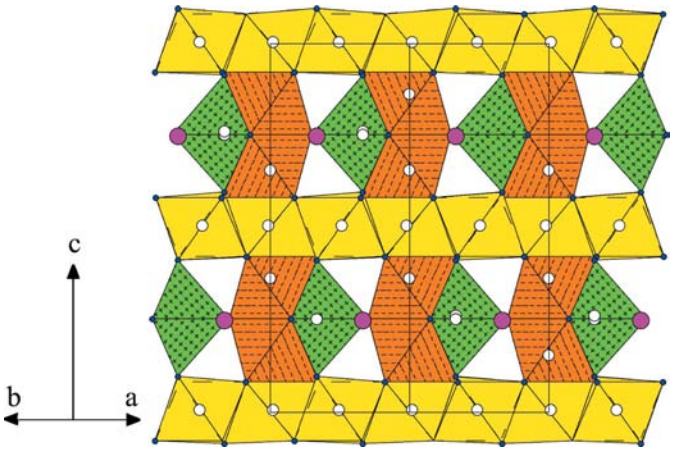

Figure 1
Schematic view of the structure of BaV_6O_{11}. Coordination polyhedra around V are indicated. White spheres represent V, spheres in magenta correspond to Ba and small blue sphere indicate oxygen positions.

Model 3: space group $P6_3mc$; 22 parameters. All coordinates were refined freely. Displacement parameters were treated as in model 2.

Additional experimental and refinement details are given in Table 1; atomic coordinates and isotropic displacement parameters are accessible through the supplementary material.[2] The internal R values as well as the final agreement factors indicate that no large systematic errors are present in the data. [This is also reflected by the F(obs)/F(calc) diagrams at the different pressures; see the supplementary material for a representative diagram.] In general, the data quality improves with increasing pressure, a fact that we attribute to the thinning out of the gasket and the consequent decrease of the gasket scattering. Although the final agreement factors are very good, not all structural parameters (*e.g.* atomic coordinates and bond lengths) follow a smooth trend as a function of pressure. The deviations from the overall observed trends at 2.19 GPa are especially pronounced. As mentioned earlier the phase transition $P6_3/mmc \rightarrow P6_3mc$ in BaV_6O_{11} involves the loss of the inversion center. As a consequence, the formation of inversion twins is likely and was indeed observed in the low-temperature study (Friese & Kanke, 2006). For the high-pressure data the number of observed Friedel pairs is low and we therefore abstained from refining a twin model for the high-pressure phase.

3. Effect of pressure on the structure of BaV_6O_{11}

3.1. Structure, equation of state and critical pressure

The structure of BaV_6O_{11} (see Fig. 1) is closely related to the magnetoplumbite structure. The O atoms, which occupy three symmetrically independent sites in the high-symmetry polymorph, form a distorted hexagonal close packing. In the ambient condition structure three symmetrically independent V sites can be distinguished. $V1O_6$ octahedra share common edges and form a regular Kagomé net normal to the hexagonal [001] direction. These layers are connected in the direction of **c** *via* $V2O_6$ octahedra, which form face-sharing dimers, and $V3O_5$ bipyramids. The Ba ions are incorporated into the cavities of this framework and are coordinated by 12 O atoms. At the phase transition the V2, as well as the O1 and O3 positions, split into two symmetrically independent positions.

Lattice parameters of BaV_6O_{11} at ambient pressure are a = 5.797 (3) and c = 13.301 (3) Å with a unit-cell volume of 387.0 (4) Å^3. The (c/a)*2/3 value of 1.530 at ambient conditions is smaller than the value of 1.633 expected for the ideal hexagonal close packing. It is remarkable that the c/a ratio in

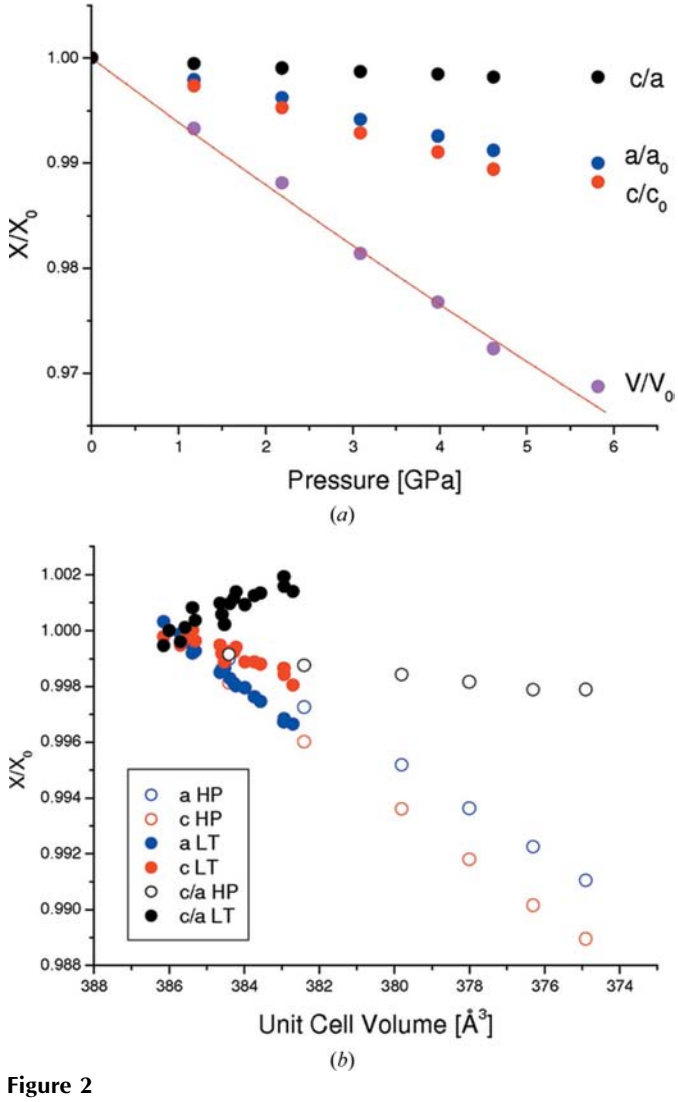

Figure 2
(*a*) Pressure dependence of the relative lattice parameters, relative c/a axial ratios and relative unit-cell volumes. The solid line is a Murnaghan equation of state fit to the compressibility data. (*b*) Relative lattice parameter and c/a ratio of BaV_6O_{11} as a function of unit-cell volume. Filled symbols represent datapoints measured as a function of temperature (Friese & Kanke, 2006), open symbols are datapoints measured as a function of pressure.

[2] Supplementary data for this paper are available from the IUCr electronic archives (Reference: EB5003). Services for accessing these data are described at the back of the journal.

$Ba^{2+}V_4^{3+}V_2^{4+}O_{11}$ is identical to that observed for $Na^{+}V_3^{3+}V_3^{4+}O_{11}$, although the valence distribution is different in the two compounds.

Fig. 2 (left) shows the relative lattice parameters of BaV_6O_{11} as a function of pressure. The compressibility data could be fitted with a Murnaghan equation of state with the zero-pressure bulk modulus $B_0 = 161$ (7) GPa and the unit-cell volume at ambient pressure $V_0 = 387.1$ (3) Å^3 (for the fixed first pressure derivative of the bulk modulus $B' = 4.00$). The bulk modulus in BaV_6O_{11} is nearly the same as in NaV_6O_{11} [$B_0 = 177$ (9) GPa]. BaV_6O_{11} is more compressible along the c axis than along the a axis. However, when compared with NaV_6O_{11} the difference in compressibility for the two directions is less pronounced in BaV_6O_{11}.

At ambient pressure and low temperature the phase transition from the centrosymmetric phase to the noncentrosymmetric phase occurs at a unit-cell volume of approximately 385 Å^3 (Friese & Kanke, 2006); according to our equation of state this volume corresponds to a pressure of approximately 0.9 GPa.

A comparison of the refinement results of the three different models described above is given in Fig. 3, which portrays the ratio of agreement factors of $R[F(\text{all})]$(Model 1)/$R[F(\text{all})]$(Model 2) (black symbols) and $R[F(\text{all})]$(Model 1)/$R[F(\text{all})]$(Model 3) (red symbols). As can be seen, at pressures above 3 GPa the overall agreement factors are clearly better for the noncentrosymmetric models (2 and 3) in space group $P6_3mc$, while below this pressure the difference for the agreement factors for the centrosymmetric and noncentrosymmetric models is not so large. Hamilton tests (Hamilton, 1965) confirm that the noncentrosymmetric models are superior at pressure above 3 GPa. On the other hand, refinements of the noncentrosymmetric model for the pressure 1.18 GPa do not lead to reasonable coordinates and interatomic distances for the heavy atoms, so that we suppose that at this pressure the sample is not yet transformed. The transition pressure thus lies in the interval $1.18 < P_c < 3.09$ GPa. This corresponds to a unit-cell volume range of $384.4\ (5) < V < 379.8\ (4)$ Å^3. The upper limit is thus at a slightly smaller unit-cell volume than that extrapolated on the basis of the low-temperature data.

Fig. 3 also demonstrates that the restricted model in $P6_3mc$ is not much worse than the unrestricted model. In addition, the coordinates of the heavy atoms V and Ba (and the corresponding interatomic distances) in the unrestricted model follow a smooth trend as a function of pressure, while the same is not true for the coordinates (and interatomic distances) of the O atoms. This indicates that our data for the high-pressure phase are of sufficient quality for the characterization of the cationic sublattice, but probably not sufficient for the determination of the oxygen coordinates in the noncentrosymmetric space group.

Fig. 2(b) shows the lattice parameters of BaV_6O_{11} as a function of unit-cell volume. The figure combines both high-

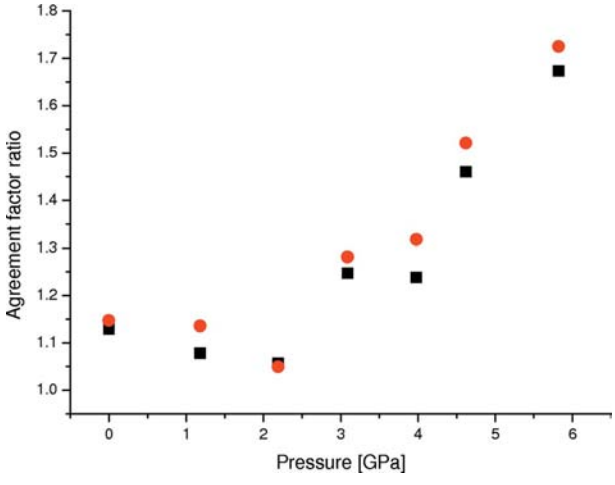

Figure 3
Agreement factor ratio R_{obs} ($P6_3/mmc$)/R_{obs} ($P6_3mc$) as a function of pressure. Black squares represent the ratio for the restricted model in $P6_3mc$ (Model 1/Model 2); red circles represent the unrestricted model (Model 1/Model 3).

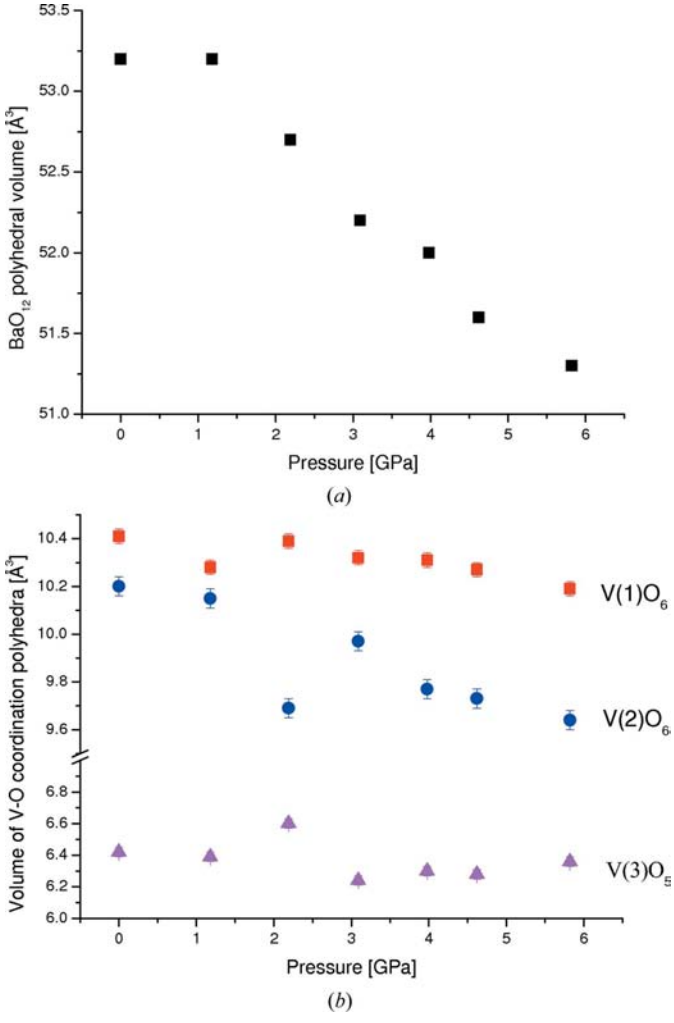

Figure 4
Pressure dependence of the polyhedral volumes in BaV_6O_{11} as calculated with the program *IVTON* (Balić-Žunić & Vickovic, 1996). Standard deviations for the polyhedral volume of BaO_{12} are smaller than the symbols.

pressure and low-temperature data, which have been taken from our earlier investigations (Friese & Kanke, 2006). It can be clearly seen from this figure that the effect of pressure and temperature on the lattice parameters of BaV_6O_{11} are different and that the induced changes cannot be attributed to a pure volume effect. While at low temperatures the *c* lattice parameter contracts less than the *a* lattice parameter, leading to a significant increase of the *c*/*a* ratio as the unit-cell volume is decreased, at high pressures the opposite behavior is observed and the *c*/*a* ratio slightly decreases as a function of the unit-cell volume. Thus, the effect of temperature is to approximate the *c*/*a* ratio to the ideal value of a hexagonal close packing, while the effect of pressure is to distort the structure even further.

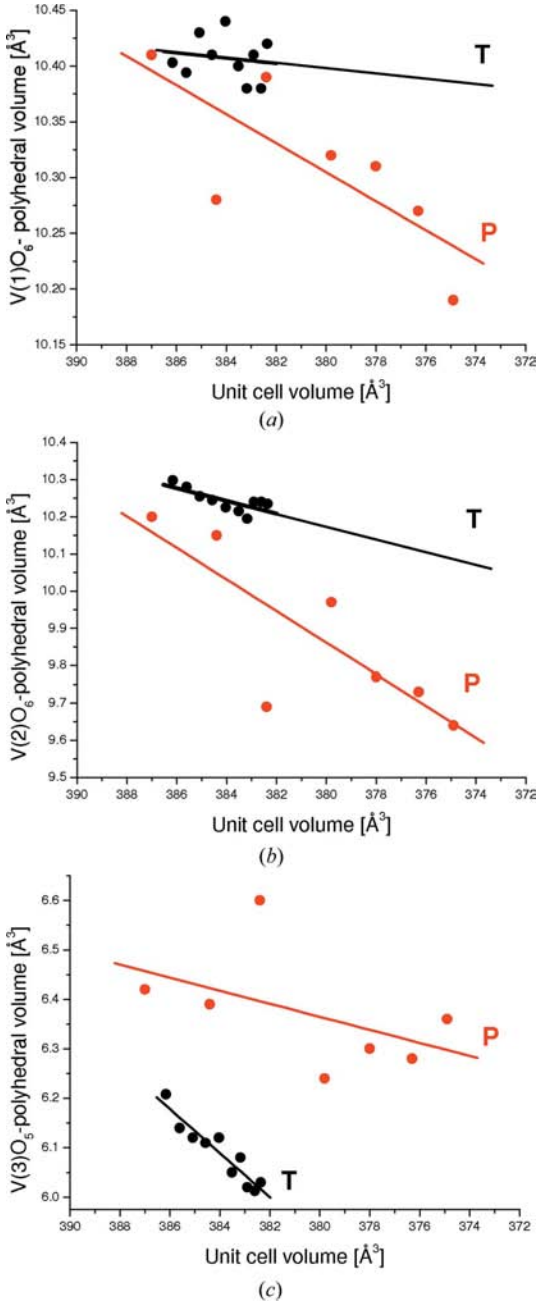

Figure 5
VO_x polyhedral volumes in BaV_6O_{11} as a function of the unit-cell volume as calculated with the program *IVTON* (Balić-Žunić & Vickovic, 1996). Black symbols correspond to datapoints as a function of temperature as given in Friese & Kanke (2006); red symbols correspond to datapoints as a function of pressure. The lines are a linear fit to the data and might serve as a guide to the eye.

This behaviour is in strong contrast to the one we observe for NaV_6O_{11} (Grzechnik *et al.*, 2008), where temperature and pressure seem to exert very similar influences on the lattice parameters of the hexagonal phases.

This difference in behavior might be related to the distinct valence distribution between the symmetrically independent V sites in both compounds and it is thus interesting to have a closer look at the VO_x coordination polyhedra.

Fig. 4 represents the polyhedra volumes for BaV_6O_{11} as a function of pressure. For the calculation we used the refined models in $P6_3/mmc$ as we considered the oxygen coordinates to be more reliable than in the noncentrosymmetric space group. Data points for the $V2O_6$ polyhedra thus represent in fact the average of two symmetrically independent octahedra in the high-pressure polymorph. As can be seen the most compressible polyhedra are the BaO_{12} and the $V2O_6$ polyhedra.[3] The volume of the $V1O_6$ octahedra decreases very slightly and the volume of the $V3O_5$ polyhedra is basically independent of pressure. A comparison with NaV_6O_{11} (Grzechnik *et al.*, 2008) reveals the following differences:

(i) In NaV_6O_{11} the compression of the NaO_{12} polyhedra saturates at approximately 2.6 GPa, while compression of the BaO_{12} polyhedron goes on even at 5.8 GPa.

(ii) In the Na-containing compound the volume of the $V1O_6$ polyhedra is almost independent of pressure, while in BaV_6O_{11} the volume slightly decreases.

(iii) The volume of $V2O_6$ in NaV_6O_{11} increases, and, in addition, the V2—V2 distances shrink on compression. In BaV_6O_{11} the $V2O_6$ polyhedra decrease on compression, while the V2—V2 distance shrinks.

(iv) The $V3O_5$ bipyramids in NaV_6O_{11} are the most compressible polyhedra. In BaV_6O_{11}, on the other hand, their volumes are almost constant. This might be related to the fact that in the Na compound the bipyramidal site is occupied by V^{4+} (Kanke *et al.*, 1992), while bond-valence calculations indicate that in the Ba compound trivalent V is incorporated into this polyhedra (Friese & Kanke, 2006).

Furthermore, the changes in the volume of the VO_x polyhedra produced by temperature or pressure in BaV_6O_{11} are distinctly different for individual polyhedra. This is evident from Fig. 5, which combines low-temperature and high-pressure data.[4]

The distinct influence of temperature and pressure is also reflected by the changes they induce in the atomic coordinates.

[3] The data corresponding to the pressure point at 2.19 GPa significantly deviate from the observed trend. We noticed this deviation for most of the geometrical parameters at this pressure point and therefore believe that the point is affected by some unidentified systematic error

[4] The datapoints as a function of pressure are rather scattered. However, taking into account that the datapoints at 2.19 GPa are most probably erroneous an overall trend can be discerned.

Fig. 6 shows the x coordinate of V1 and the z coordinate of V3 as a function of the unit-cell volume. As has been shown in Grzechnik *et al.* (2008) these two coordinates are related to the two most important contributions of individual primary modes to the overall structural distortions in the phase transition.

In this context it should be mentioned that the temperature-induced transitions $P6_3/mmc \rightarrow P6_3mc$ in the AV_6O_{11} family are accompanied by paramagnetic–paramagnetic transitions. For NaV_6O_{11} a spin-singlet state involving the V1 ions in the Kagomé net has been confirmed for the $P6_3mc$ phase at lower temperatures (Uchida *et al.*, 2001). This is reflected by the fact that in the low-temperature polymorphs the regular Kagomé net formed by V1 ions is broken. As the V1 atoms shift from their special positions [$(\frac{1}{2},0,0)$ in $P6_3/mmc$ to the more general position $(x,2x,0)$ in $P6_3mc$], V1 trimers are formed and the V1—V1 distances split into inter-trimer and intra-trimer distances. Fig. 7 shows the V1—V1 distances in BaV_6O_{11} as a function of the unit-cell volume.

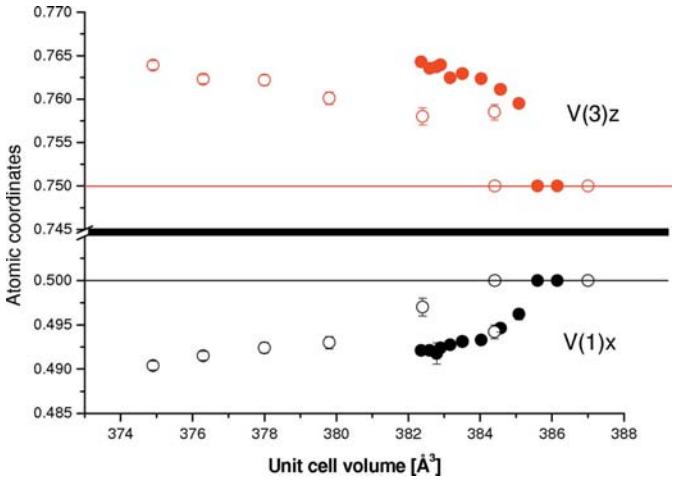

Figure 6
V1x and V3z coordinate as a function of the unit-cell volume. Filled symbols correspond to datapoints as a function of temperature as given in Friese & Kanke (2006); open symbols correspond to datapoints as a function of pressure. For the pressure point at 1.18 GPa coordinates are represented for the models in the space group $P6_3/mmc$ and $P6_3mc$.

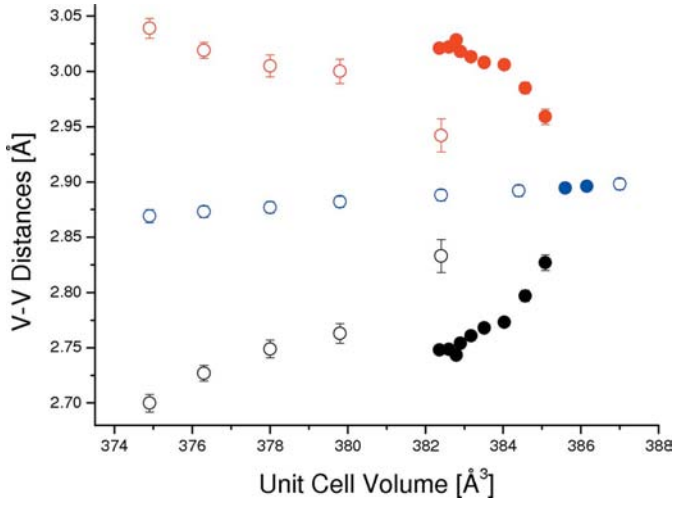

Figure 7
V1—V1 distances in the Kagomé net as a function of the unit-cell volume. Filled symbols represent distances corresponding to the low-temperature study published in Friese & Kanke (2006), while open symbols represent distances as a function of pressure. Blue symbols are V—V distances obtained from refinements in the space group $P6_3/mmc$ (Model 1), while red and black symbols correspond to refinements in the space group $P6_3mc$.

From Figs. 6 and 7 it is evident that both the coordinates and the splitting into inter-trimer and intra-trimer distances within the Kagomé net follow different trends as a function of temperature than as a function of pressure. This observation is in strong contrast to the uniform behavior of these parameters with varying pressure/temperature in NaV_6O_{11} (Grzechnik *et al.*, 2008).

One can thus say that the observed phase transition in NaV_6O_{11} could be explained as a pure volume effect, while for BaV_6O_{11} other factors have to be taken into account. In NaV_6O_{11} the lattice parameters a and c are uniquely determined for a given unit-cell volume, while in the Ba compound they vary in the P–T diagram. This suggests that the latter compound has one more free parameter to define the unit cell.

On the basis of our observations we believe that this additional degree of freedom is closely related to the valence distribution among the symmetrically independent vanadium sites. In NaV_6O_{11} the change in valence induced by temperature or pressure seems to be restricted to the V2 and V3 sites. In BaV_6O_{11}, on the other hand, the V1 site is most probably also involved in the valence fluctuations.

4. Conclusions

According to our results BaV_6O_{11} undergoes a structural phase transition $P6_3/mmc \rightarrow P6_3mc$ below 3 GPa. The transition is exclusively reflected in subtle changes of the diffraction intensities and not accompanied by splitting of reflections or the appearance of additional reflections in the diffraction diagram.

The pressure-induced transition in BaV_6O_{11} takes place at a smaller critical unit-cell volume when compared with the transition at low temperatures. While in the Na-containing compound the transition can be explained as a pure volume effect, in BaV_6O_{11} an additional degree of freedom has to be taken into account. The difference in the behaviour of the two compounds might be related to the more flexible valence distribution in BaV_6O_{11} when compared with NaV_6O_{11}.

Further investigations on the high-pressure behavior of other representatives of the family AV_6O_{11} and experiments varying temperature and pressure simultaneously could shed more light on the underlying mechanisms of the phase transition observed.

Financial support by the Ministerio de Ciencia y Innovación (FIS2008-03834, FIS2005-04476, FIS2005-07090), the Gobierno Vasco, and the Universidad del País Vasco is acknowledged.

References

Akiba, A., Yamada, H., Matsuo, R., Kanke, Y., Haeiwa, T. & Kita, E. (1998). *J. Phys. Soc. Jpn*, **67**, 1303–1305.

Angel, R. J. (2006). *Absorb*, Version 6.1. Virginia Tech University, Blacksburg, Virginia, USA.

Balić Žunić, T. & Vicković, I. (1996). *J. Appl. Cryst.* **29**, 305–306.

Boehler, R. (2006). *Rev. Sci. Instrum.* **77**, 115103.

Boehler, R. & de Hantsetters, K. (2004). *High Press. Res.* **24**, 391–396.

Friese, K. & Kanke, Y. (2006). *J. Solid State Chem.* **179**, 3277–3285.

Grzechnik, A., Kanke, Y. & Friese, K. (2008). *J. Phys. Condens. Matter*, **20**, 285208.

Hamilton, W. C. (1965). *Acta Cryst.* **18**, 866–870.

Hata, Y., Kanke, Y., Kita, E., Suzuki, H. & Kido, G. (1999). *J. Appl. Phys.* **85**, 4768–4770.

Kanke, Y. (1999). *Phys. Rev. B*, **60**, 3764–3776.

Kanke, Y., Izumi, F., Morii, Y., Akiba, E., Funahashi, S., Kato, K., Isobe, M., Takayama-Muromachi, E. & Uchida, Y. (1994). *J. Solid State Chem.* **112**, 429–437.

Kanke, Y., Izumi, F., Takayama-Muromachi, E., Kato, K., Kamiyama, T. & Asano, H. (1991). *J. Solid State Chem.* **92**, 261–272.

Kanke, Y., Kato, K., Takayama-Muromachi, E. & Isobe, M. (1992). *Acta Cryst.* C**48**, 1376–1380.

Kato, H., Kato, M., Yoshimura, K. & Kosuge, K. (2001). *J. Phys. Condens. Matter*, **13**, 9311–9333.

Mentre, O. & Abraham, F. (1996). *J. Solid State Chem.* **125**, 91–101.

Mentre, O., Kanke, Y., Dhaussy, A.-C., Conflant, P., Hata, Y. & Kita, E. (2001). *Phys. Rev. B*, **64**, 174404.

Petříček, V., Dušek, M. & Palatinus, L. (2006). *JANA*2006. Institute of Physics, Academy of Sciences, Praha, Czech Republic.

Piermarini, G. J., Block, S. & Barnett, J. D. (1973). *J. Appl. Phys.* **44**, 5377–5382.

Roy, M. E. de, Besse, J. P., Chevalier, R. & Gasperin, M. (1987). *J. Solid State Chem.* **67**, 185–189.

Stoe & Cie (1999). *X-SHAPE*, Revision 1.06. Stoe & Cie GmbH, Darmstadt, Germany.

Stoe & Cie (2006). *X-AREA*: Stoe IPDS Software, Version 1.39. Stoe & Cie GmbH, Darmstadt, Germany.

Uchida, Y., Onoda, M. & Kanke, Y. (2001). *J. Magn. Magn. Mater.* **226**, 446–448.